

# A mass-flux cumulus parameterization scheme for large-scale models: description and test with observations

Tongwen Wu

Received: 14 August 2010 / Accepted: 11 January 2011 / Published online: 28 January 2011  
© Springer-Verlag 2011

**Abstract** A simple mass-flux cumulus parameterization scheme suitable for large-scale atmospheric models is presented. The scheme is based on a bulk-cloud approach and has the following properties: (1) Deep convection is launched at the level of maximum moist static energy above the top of the boundary layer. It is triggered if there is positive convective available potential energy (CAPE) and relative humidity of the air at the lifting level of convection cloud is greater than 75%; (2) Convective updrafts for mass, dry static energy, moisture, cloud liquid water and momentum are parameterized by a one-dimensional entrainment/detrainment bulk-cloud model. The lateral entrainment of the environmental air into the unstable ascending parcel before it rises to the lifting condensation level is considered. The entrainment/detrainment amount for the updraft cloud parcel is separately determined according to the increase/decrease of updraft parcel mass with altitude, and the mass change for the adiabatic ascent cloud parcel with altitude is derived from a total energy conservation equation of the whole adiabatic system in which involves the updraft cloud parcel and the environment; (3) The convective downdraft is assumed saturated and originated from the level of minimum environmental saturated equivalent potential temperature within the updraft cloud; (4) The mass flux at the base of convective cloud is determined by a closure scheme suggested by Zhang (J Geophys Res 107(D14), doi:10.1029/2001JD001005, 2002) in which the increase/decrease of CAPE due to changes of the thermodynamic states in the

free troposphere resulting from convection approximately balances the decrease/increase resulting from large-scale processes. Evaluation of the proposed convection scheme is performed by using a single column model (SCM) forced by the Atmospheric Radiation Measurement Program's (ARM) summer 1995 and 1997 Intensive Observing Period (IOP) observations, and field observations from the Global Atmospheric Research Program's Atlantic Tropical Experiment (GATE) and the Tropical Ocean and Global Atmosphere Coupled Ocean–Atmosphere Response Experiment (TOGA COARE). The SCM can generally capture the convective events and produce a realistic timing of most events of intense precipitation although there are some biases in the strength of simulated precipitation.

**Keywords** Mass-flux cumulus parameterization scheme · Large-scale model · Single column model · Test with observations

## 1 Introduction

Cumulus convection is a key process in controlling water vapor content of the atmosphere. The heat release from condensation in convective processes is a dominant component of the atmosphere's energy budget (Emanuel et al. 1994). Climate models should take into account collective influence of small-scale convective processes on large-scale variables in each model grid box. Current climate models cannot resolve convective-scale and explicitly predict convections, thus effects of convections on the resolved scales must be parameterized.

The idea of cumulus parameterization was born in the early 1960s. It was introduced by Charney and Eliassen (1964) and Ooyama (1964) in tropical cyclone modeling

---

T. Wu (✉)  
National Climate Center (Beijing Climate Center),  
China Meteorological Administration (CMA),  
46 Zhongguancun Nandajie, 100081 Beijing,  
People's Republic of China  
e-mail: twwu@cma.gov.cn

and by Manabe et al. (1965) in a general circulation model. Since then, a number of cumulus parameterization schemes have been developed for comprehensive numerical weather prediction (NWP) and climate models, to take into account the subgrid-scale characteristics of latent heat release and mass transport associated with convective clouds, and to accurately predict rainfall, especially for heavy rain episodes (e.g., Arakawa and Schubert 1974; Anthes 1977; Kuo and Raymond 1980; Fritsch and Chappell 1980; Betts and Miller 1986; Tiedtke 1989; Gregory and Rowntree 1990; Kain and Fritsch 1990; Emanuel 1991; Donner 1993; Grell 1993; Zhang and McFarlane 1995; Wang and Randall 1996; Sun and Haines 1996; Hu 1997). Many of these schemes continue to be improved (e.g., Janjic 1994; Cheng and Arakawa 1997; Emanuel and Zivkovic-Rothman 1999; Gregory et al. 2000; Grell and Devenyi 2002). As reviewed in Arakawa (2004) and Bechtold (2006), these parameterization schemes can be regrouped into three classes: (1) “Kuo” schemes based on moisture budgets (e.g., Kuo 1965; Kuo 1974); (2) Adjustment schemes including moist convective adjustment (e.g., Manabe et al. 1965) and penetrative adjustment scheme (e.g., Betts and Miller 1986); (3) Mass flux schemes which include multiple entraining plumes—spectral model, single entraining/detraining plume—bulk model, and episodic mixing scheme (e.g., Emanuel 1991; Gregory 1997; Emanuel and Zivkovic-Rothman 1999). The first two classes simulate the effects of convection by adjusting the lapse rates of both temperature and moisture to a specified reference profile at each grid point (without attempting to simulate the explicit convective process). Mass flux schemes do attempt to explicitly formulate and account for convective processes at each grid point.

In addition to ‘traditional’ convection parameterizations, a cloud-resolving approach (also called “super-parameterization”) was proposed by Grabowski (Grabowski and Smolarkiewicz 1999; Grabowski 2001) that would be another pathway to solve the cumulus problem.

At present, the mass flux approach is still widely used in weather and climate models as it has a stronger physical basis, in comparison to the earlier empirical adjustment methods (e.g., moist convective adjustment and Kuo-type schemes) and provides an understanding of how convection affects the large-scale atmosphere. However, mass flux schemes are much more complex and require additional assumptions. Some relevant problems still exist:

1. The most difficult issue is to locate convection. The physical processes initiating convection are not well understood. There is no general criterion to decide when burst out of convection should take place, i.e., when to allow a moist convective parcel to overcome the stable layer at cloud base and to have access to the convective available potential energy (CAPE). It has been shown that some simulations are highly sensitive to the triggering function used (e.g., Kain and Fritsch 1990; Stensrud and Fritsch 1994).
2. Cloud profiles are highly sensitive to the entrainment/detrainment cloud model. One of the most important problems is the treatment of entrainment of environmental air into cloud columns (Arakawa 2004; Deb et al. 2006; Wang et al. 2007). The entrainment and detrainment rates are commonly specified by certain hypothesis such as constant, a designated function of altitude (e.g., Tiedtke 1989), a velocity-dependent rate (Neggers et al. 2002), an inverse-height relationship (Jakob and Siebesma 2003; Zhang 2009), a function with parcel buoyancy and inversely as the square of the updraft speed (Gregory 2001) or decreasing over the course of the day (Grabowski et al. 2006), or parameterized with a characteristic fractional entrainment rate (e.g., Zhang and McFarlane 1995) or based on tropospheric environmental humidity and subsaturation (Bechtold et al. 2008).

This paper is to develop and validate a new mass-flux approach to parameterize deep convection. It functions as a bulk type scheme which resembles to existing frameworks, essentially the rather general framework proposed by Tiedtke (1989) and Zhang and McFarlane (1995). Its main distinctness from commonly used schemes is: (1) The entrainment of the lateral environment air below the cloud base is involved. Almost every convection scheme that works with a plume model neglects the mixing of the ascent parcel with the environment air in the sub-cloud layer. The importance of the sub-cloud layer in the parameterization of moist convection has been recognized (Jakob and Siebesma 2003) and its effects on weather and climate seem to be rather significant; (2) entrainment and detrainment in convective updrafts are not prescribed as a function of altitude but fully determined by the change of the updraft cloud package mass with altitude and is dependent on properties of the upward cloud parcel and the environment air and the mass flux at the cloud base.

The structure of this paper is as follows: A detailed description of the convection scheme is presented in Sect. 2. Its evaluation with a single column model (SCM) and observational data is given in Sect. 3. Section 4 contains summary and concluding remarks.

## 2 Design of cumulus parameterization scheme

The cumulus parameterization in this work is to represent the collective effect of cumulus clouds without predicting individual clouds. The convective updrafts and downdrafts

associated with moist air and water phase changes are included.

### 2.1 Triggering of convection

The cumulus clouds are assumed to be embedded in the large-scale environment, and have a common cloud base. Similar to Zhang and McFarlane (1995), the first step in the scheme is to find the bottom of the unstable layer in the lower troposphere, that is the level at which the moist static energy reaches its first maximum from the top of the boundary layer to 700 hPa. Also this level is the initial lifting level of a convective cloud parcel, and is limited to below 700 hPa based on consideration that mid-latitude convection, especially at night time, might root at upper atmospheric levels. This parcel is then assumed to undergo dry adiabatic ascent from its lifting base (*LB*). The second step is to determine the cloud base i.e., the lifting condensation level (*LCL*) that is the lowest level at which the adiabatic parcel becomes supersaturated. Once cloud base detected, the cloud parcel rises under moist adiabatic processes to the cloud top level (*CTL*) which is defined as the level at which the buoyancy of an air parcel becomes negative, i.e., the ‘level of zero buoyancy’ where the virtual potential temperature of the air parcel and that of the environment become equal to each other.

The convection is activated when (1) the environmental air in the updraft source layer is sufficiently moist and the relative humidity at the level of undiluted parcel lifting bottom (*LB*) is assumed in excess of 75% (which depends on the grid horizontal resolutions while it is used in GCMs), and (2) the convective available potential energy (*CAPE*) must be greater than zero. The *CAPE* is defined as the vertical integration of the buoyancy between the *LB* and the *CTL*:

$$CAPE \equiv \int_{z_{LB}}^{z_{CTL}} F_B dz = R_d \int_{p(z_{CTL})}^{p(z_{LB})} [(T_c)_v - \bar{T}_v] d \ln p \quad (1)$$

where  $R_d$  is the gas constant of dry air.  $z_{LB}$  and  $z_{CTL}$  are the heights of an air parcel at its *LB* and *CTL*, respectively. The overbar denotes the environmental variables.  $(T_c)_v$  is the virtual temperature of the adiabatic ascending cloud and is computed by  $(T_c)_v = T_c(1 + 0.608q_{LB})/(1.0 + q_{LB})$  below its lifting condensation level and  $(T_c)_v = T_c[1 + 1.608q^*(T_c)]/(1 + q^* + q_1)$  above its *LCL*. Here  $q^*(T_c)$  is the saturated water-vapor mixing ratio with the undiluted parcel temperature  $T_c$ .  $q_1$  is the total condensate and given by  $q_1 = q_{LCL} - q^*(T)$  for moist-adiabatic ascent. In the expression (1), no mixing of the parcels with the environment has been taken into account, i.e., the ascent is supposed to be adiabatic (no mass and energy is exchanged

with the environment). The numerical formalism to compute the properties of the adiabatic ascent parcel are given in the ‘‘Appendix’’.

Convective downdraft plays an essential role in atmospheric convection. The downdraft plume is originated at the level of free sink (*LFS*) which is defined as the level of minimum environmental saturated equivalent potential temperature  $\theta_{se}$  between the *LCL* and the *CTL*. The downdraft parcel is assumed to be completely saturated above cloud base and is terminated if it becomes warmer than its environment or if it reaches the surface and if no water is evaporated.

### 2.2 Basic equations for large-scale convective tendencies

The basic equations for the large-scale convective tendencies due to contribution of cumulus convection to the large-scale budgets of heat, moisture and momentum are expressed in terms of bulk convective fluxes as followings (e.g., Tiedtke 1989; Zhang and McFarlane 1995):

$$c_p \left( \frac{\partial \bar{T}}{\partial t} \right)_{cu} = -\frac{1}{\rho} \frac{\partial}{\partial z} [M_u(s_u - \bar{s}) + M_d(s_d - \bar{s})] + L(c_u - e_d - e_l), \quad (2)$$

$$\left( \frac{\partial \bar{q}}{\partial t} \right)_{cu} = -\frac{1}{\rho} \frac{\partial}{\partial z} [M_u(q_u - \bar{q}) + M_d(q_d - \bar{q})] - (c_u - e_d - e_l), \quad (3)$$

$$\left( \frac{\partial \bar{u}}{\partial t} \right)_{cu} = -\frac{(1 - k_u)}{\rho} \frac{\partial}{\partial z} [M_u(u_u - \bar{u}) + M_d(u_d - \bar{u})], \quad (4)$$

$$\left( \frac{\partial \bar{v}}{\partial t} \right)_{cu} = -\frac{(1 - k_u)}{\rho} \frac{\partial}{\partial z} [M_u(v_u - \bar{v}) + M_d(v_d - \bar{v})], \quad (5)$$

for  $z \geq z_{LB}$ . Below the *LB* ( $z_s < z < z_{LB}$  where  $z_s$  is the surface height), the Eqs. 2–5 are expressed as

$$c_p \left( \rho \frac{\partial \bar{T}}{\partial t} \right)_{cu} = -\frac{1}{(z_{LB} - z_s)} (M_u[s(z_{LB}) - s_u(z_{LB})] + M_d[s(z_{LB}) - s_d(z_{LB})]) \quad (6)$$

$$\left( \rho \frac{\partial \bar{q}}{\partial t} \right)_{cu} = -\frac{1}{(z_{LB} - z_s)} (M_u[q(z_{LB}) - q_u(z_{LB})] + M_d[q(z_{LB}) - q_d(z_{LB})]), \quad (7)$$

$$\left( \frac{\partial \bar{u}}{\partial t} \right)_{cu} = -\frac{(1 - k_u)}{(z_{LB} - z_s)} (M_u[u_u(z_{LB}) - \bar{u}(z_{LB})] + M_d[u_d(z_{LB}) - \bar{u}(z_{LB})]), \quad (8)$$

$$\left( \frac{\partial \bar{v}}{\partial t} \right)_{cu} = -\frac{(1 - k_u)}{(z_{LB} - z_s)} (M_u[v_u(z_{LB}) - \bar{v}(z_{LB})] + M_d[v_d(z_{LB}) - \bar{v}(z_{LB})]). \quad (9)$$

The subscript ‘‘u’’ and ‘‘d’’ denotes the variables for updraft and downdraft cloud plumes, respectively. The

overbar “-” indicates environmental variable.  $T$ ,  $q$ ,  $u$ , and  $v$  are temperature, water-vapor mixing ratio, zonal and meridional winds, respectively.  $M_u(z)$  and  $M_d(z)$  are the upward mass flux for the updraft and downdraft plumes, respectively.  $c_u$  and  $e_d$  denote the condensation rate in the updraft and the evaporation rate of precipitation in the downdraft, respectively.  $k_u$  is an empirical constant and set to 0.7 (refer to Gregory et al. 1997).  $e_l$  represents the evaporation rate of cloud water that has been detrained into the environment. A Sundqvist (1988) style evaporation of the convective precipitation is introduced to parameterize  $e_l$  (see Collins et al. 2004) as

$$e_l = K_e (1 - \overline{RH}) \cdot G_p^{1/2}, \quad (10)$$

where  $\overline{RH}$  is the relative humidity,  $G_p$  denotes the conversion of cloud water to precipitation. The coefficient  $K_e$  takes a value of  $2.0 \times 10^{-4} (\text{kg m}^{-2} \text{s}^{-1})^{-1/2} \text{s}^{-1}$ . The variable  $e_l$  has units of  $\text{s}^{-1}$ . Then, the rain water flux at height  $z$  can be expressed as

$$P(z) = \int_z^\infty (G_p - e_l - e_d) \bar{\rho} dz. \quad (11)$$

### 2.3 Updraft

The cloud mass flux  $M_u(z)$  and the condensation  $c_u$  in the updraft are commonly formulated in a bulk entraining–detraining plume model. The budget equations for mass, dry static energy, moisture, cloud liquid water, and momentum for an ensemble of updraft cloud package are commonly expressed as (e.g., Tiedtke 1989; Zhang and McFarlane 1995):

$$\frac{\partial M_u}{\partial z} = E_u - D_u \quad (12)$$

$$\frac{\partial}{\partial z} (M_u s_u) = E_u s_u - D_u \bar{s} + \rho L c_u \quad (13)$$

$$\frac{\partial}{\partial z} (M_u q_u) = E_u q_u - D_u \bar{q}^* - \rho c_u \quad (14)$$

$$\frac{\partial}{\partial z} (M_u \ell_u) = -D_u \bar{\ell}_u + \rho c_u - \rho G_p \quad (15)$$

$$\frac{\partial}{\partial z} (M_u u_u) = E_u u_u - D_u \bar{u} \quad (16)$$

$$\frac{\partial}{\partial z} (M_u v_u) = E_u v_u - D_u \bar{v} \quad (17)$$

where  $E$  denotes entrainment,  $D$  detrainment,  $s = c_p T + gz$  the dry static energy,  $\rho$  the air density,  $l$  the cloud water mixing ratio, and  $c_u$  the release of latent heat from condensation.

It is well-known that clouds with various sizes may, at the same time, exist in a given GCM grid box. In this scheme, all

deep convective cloud bases are assumed to be located at the same level. So, all individual clouds in the same grid box that undergo dry adiabatic and then moist adiabatic ascent must share common thermodynamic properties such as temperature  $T_c(z)$  and moisture  $q_c(z)$ . At any given level  $z$  between the cloud base and cloud top, although there may exist detrainment/entrainment from some clouds and then be entrained/detrained into other clouds, only influences of the net entrainment from the environment or net detrainment from the ensemble package of updraft clouds to the environmental air are considered in this scheme, namely,

$$E_u = \frac{\partial M_u}{\partial z} \quad \text{and} \quad D_u = 0, \quad \text{for} \quad \frac{\partial M_u}{\partial z} > 0; \quad (18)$$

or,

$$D_u = -\frac{\partial M_u}{\partial z} \quad \text{and} \quad E_u = 0 \quad \text{for} \quad \frac{\partial M_u}{\partial z} < 0. \quad (19)$$

It implies that the entrainment  $E_u(z)$  or detrainment  $D_u(z)$  in Eq. 12 fully depends on the change of the upward mass flux  $M_u(z)$  with altitude.

$M_u(z)$  is parameterized as following. As for a collection of undiluted moist adiabatic ascent clouds, its temperature and humidity change separately from  $T_c$  to  $T_c + dT_c$  and from  $q_c$  to  $q_c + dq_c$  when it rises from  $z$  to  $z + dz$  where the corresponding pressure changes from  $p_c$  to  $p_c + dp_c$ . The cloud parcel will have gain/loss of internal energy during its ascent motion as:

$$(\delta Q)_{cld} = m_c \left( c_p dT_c - \frac{RT_{v,c}}{p_c} dp_c \right) + m_c L dq_c. \quad (20)$$

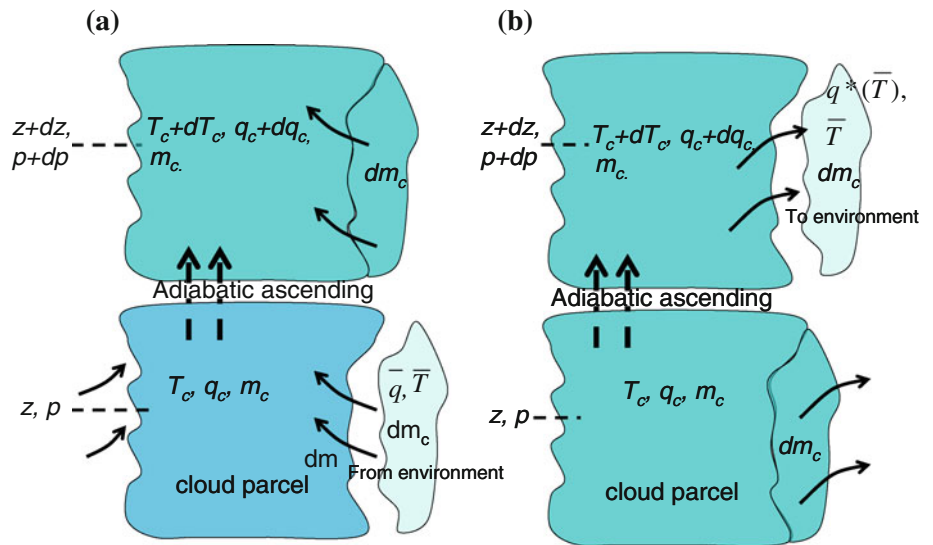
where,  $m_c$  is the undiluted cloud mass and  $p_c$  pressure in cloud. The first term in the right side of Eq. 20 represents the internal energy increment and the second term denotes the obtained latent heat energy due to humidity change  $dq_c$  of the saturated cloud parcel.

As shown by the schematic in Fig. 1, when the environmental air is entrained into the updraft cloud or the cloud air is detrained into the environment, the cloud mass will change from  $m_c(z)$  to  $m_c(z) + dm_c$ . Here,  $dm_c > 0$  means the entrainment of the environmental air into the updraft cloud and  $dm_c < 0$  denotes the detrainment of updraft cloud into the environment. Then, the gain/lose internal energy by the updraft cloud pack in the expression (20) will be changed to

$$(\delta Q)_{cld} = m_c \left( c_p dT_c - \frac{RT_{v,c}}{p_c} dp_c \right) + m_c L dq_c + c_p T_c dm_c + L q_c dm_c. \quad (21)$$

In the same time, the environment must lose (or gain) internal thermal energy  $c_p \bar{T} dm_c$ , and latent heat  $L \bar{q} dm_c$  when  $dm_c > 0$  (or  $dm_c < 0$ ). The total energy loss/gain for the environment can be rewritten as

**Fig. 1** Schematic diagram of **a** entrainment and **b** detrainment for an ensemble of updraft cloud parcels



$$(\delta Q)_{env} = c_p \bar{T} dm_c + L \bar{q} dm_c. \tag{22}$$

The cloud and environment are together composed of an adiabatic system, and the  $(\delta Q)_{env}$  must balance the  $(\delta Q)_{clad}$ . That is

$$c_p \bar{T} dm_c + L \bar{q} dm_c = m_c \left( c_p dT_c - \frac{RT_{v,c}}{p_c} dp_c \right) + m_c L dq_c + c_p T_c dm_c + L q_c dm_c, \tag{23}$$

or

$$c_p (\bar{T} - T_c) dm_c + L (\bar{q} - q_c) dm_c = m_c \left( c_p dT_c - \frac{RT_{v,c}}{p_c} dp_c \right) + m_c L dq_c. \tag{24}$$

The parcel pressure  $p_c$  is commonly equal to the environmental pressure  $\bar{p}$  and there exists a relation  $dp_c = d\bar{p}$ . It is known that the large-scale environmental air approximately satisfies the hydrostatic balance, i.e.,

$$d\bar{p} = -\frac{\bar{p}}{RT_v} g dz. \tag{25}$$

Now, we introduce the moist static energy of the ascent parcel  $h_c = c_p T_c + gz + Lq_c$  and the moist static energy of the environmental air  $\bar{h} = c_p \bar{T} + gz + L\bar{q}$ , respectively. Equation 24 can be rewritten as

$$(\bar{h} - h_c) \frac{dm_c}{m_c dz} = g \frac{T_{v,c}}{\bar{T}_v} + L \frac{dq_c}{dz} + c_p \frac{dT_c}{dz}. \tag{26}$$

Only  $m_c(z)$  in Eq. 26 is an unknown variable. Its solution can be expressed as

$$m_c(z + dz) = m_c(z) e^{\lambda(z) \cdot dz}, \tag{27}$$

where

$$\lambda(z) \equiv \frac{g \frac{T_{v,c}}{\bar{T}_v} + L \frac{dq_c}{dz} + c_p \frac{dT_c}{dz}}{\bar{h} - h_c}. \tag{28}$$

Here, the variables with subscript “c” denote the temperature and water vapor mixing ratio only for moist adiabatic ascent cloud parcel.

It is noted that the updraft mass flux  $M_u(z)$  is defined as the net upward mass of cloud parcel  $m_c$  across the height  $z$  at a given time interval. So, there is a similar relationship to the expression (27) as

$$M_u(z + dz) = M_u(z) e^{\lambda(z) \cdot dz} \tag{29}$$

or,

$$M_u(z) = M_b(z_{LB}) e^{\lambda(z) \cdot (z - z_{LB})}, \tag{30}$$

where  $M_b(z_{LB})$  is the mass flux at  $LB$ . Following Eq. 30, there is  $\frac{\partial M_u(z)}{\partial z} = M_u(z) \cdot \lambda(z)$ . So  $\lambda(z)$  represents the strength of entrainment when  $\lambda(z) > 0$  or detrainment when  $\lambda(z) < 0$ .

In Eqs. 13 and 14  $s_u$  (or  $T_u$ ) and  $q_u$  are different from  $s_c$  (or  $T_c$ ) and  $q_c$ . The variables with subscript “u” already include influences of condensation and entrainment or detrainment mixing with the environment. Based on Eqs. 13 and 14, there is

$$\frac{\partial}{\partial z} (M_u h_u) = E_u h_u - D_u \bar{h}^*, \tag{31}$$

where

$$h_u \equiv s_u + Lq_u = c_p T_u + gz + Lq_u \tag{32}$$

is wet static energy of the updraft cloud and can be directly solved from Eq. 31. With the aid of relationship

$$q_u = q^*(T_u), \tag{33}$$

i.e., the updraft cloud is always saturated after condensation and mixing processes. So,

$$[c_p T_u + gz + Lq^*(T_u)] - h_u = 0. \tag{34}$$

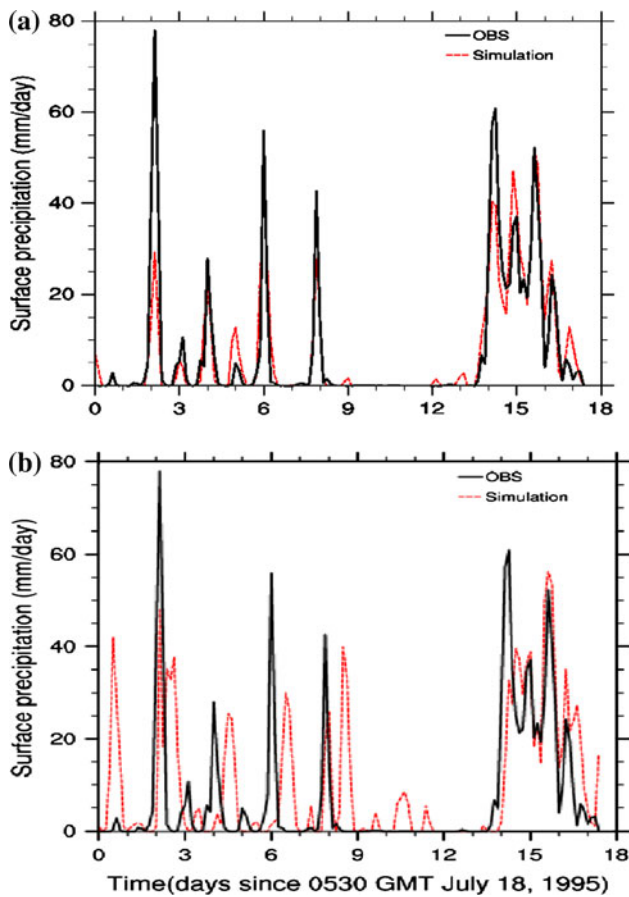


**Fig. 2** Time series of observed and simulated surface precipitation rates during summer 1995 IOP from the SCM using **a** Wu's scheme and **b** Zhang–McFarlane'95 scheme

$T_u$  can be estimated from Eq. 34 by using Newton–Raphson iteration.

Equation 15 implies that fractional condensed water is converted to precipitation and the remainder will become cloud water and contribute to moistening the environment. Following Lord et al. (1982), the conversion from cloud droplets to raindrops is assumed to be proportional to the liquid cloud water content and the upward mass flux as

$$\rho G_p = c_0 M_u \cdot l_u, \quad (35)$$

where constant  $c_0$  is related to horizontal resolution and  $c_0 = 6 \times 10^{-3} \text{ m}^{-1}$  for T42 resolution of the Beijing Climate Center Atmospheric General Circulation Model (BCC\_AGCM2.0.1, Wu et al. 2010) in this work.

If the mass flux at the cloud base  $M_b$  is known, the unknown variables such as  $M_u$ ,  $E_u$ ,  $D_u$ ,  $l_u$ ,  $c_u$ ,  $u_u$ , and  $v_u$  can be calculated.

#### 2.4 Downdraft

Similar to the updraft, vertical distributions of the downdraft mass flux, dry static energy and moisture below the

$LFS$  are determined by the equations for mass, dry static energy, moisture content, and momentum:

$$\frac{\partial M_d}{\partial z} = E_d - D_d \quad (36)$$

$$\frac{\partial M_d s_d}{\partial z} = E_d \bar{s} - D_d s_d + L \bar{\rho} e_d \quad (37)$$

$$\frac{\partial M_d q_d}{\partial z} = E_d \bar{q} - D_d q_d - \bar{\rho} e_d \quad (38)$$

$$\frac{\partial M_d u_d}{\partial z} = E_d \bar{u} - D_d u_d \quad (39)$$

$$\frac{\partial M_d v_d}{\partial z} = E_d \bar{v} - D_d v_d \quad (40)$$

In which  $e_d$  is the evaporation of convective rain to maintain a saturated descent, moisten and cool the environmental air.

The magnitude of the downdraft mass flux at the  $LFS$  is specified as a simple function of updraft mass flux and relative humidity.

$$M_d(z_{LFS}) = -\beta(1 - \overline{RH}_{LFS}) \cdot M_u(z_{LFS}) \quad (41)$$

where  $\overline{RH}_{LFS}$  is the mean (fractional) relative humidity at the  $LFS$  and  $\beta = 2$  is an empirical coefficient (Knupp and Cotton 1985; Tompkins 2001). The detrainment from the downdraft is assumed to be confined to the sub-cloud layer. In this work, the downdraft mass flux  $M_d(z)$  takes the form similar to the scheme of Zhang and McFarlane (1995) as

$$M_d(z) = \alpha \cdot M_d(z_{LFS}) \frac{e^{\lambda_d \cdot (z_{LFS} - z)} - 1}{\lambda_d \cdot (z_{LFS} - z)} \quad (42)$$

In the scheme,  $\lambda_d$  ( $5 \times 10^{-4} \text{ m}^{-1}$ ) is an empirical coefficient and  $\alpha$  is a “proportionality factor” to ensure that the downdraft strength is physically consistent with precipitation availability taking the form of

$$\alpha = \frac{P}{P + E_d}, \quad (43)$$

where  $P$  is the total precipitation in the convective cloud column. This formalism ensures that the downdraft mass flux vanishes in the absence of precipitation, and that evaporation cannot exceed the precipitation. With the aid of Eqs. 37 and 38, there is

$$\frac{\partial M_d h_d}{\partial z} = E_d \bar{h} - D_d h_d. \quad (44)$$

The moist static energy for downdraft air  $h_d = s_d + Lq_d$  can be computed. The downdraft air is assumed saturated. Then  $s_d$  and  $q_d \equiv q^*(T_d, p)$  can be approximately calculated by an iterative error function similar to Eq. 34.

#### 2.5 Closure

Based on observational studies, Zhang (2002) proposed a closure scheme that assumes that stabilization of the

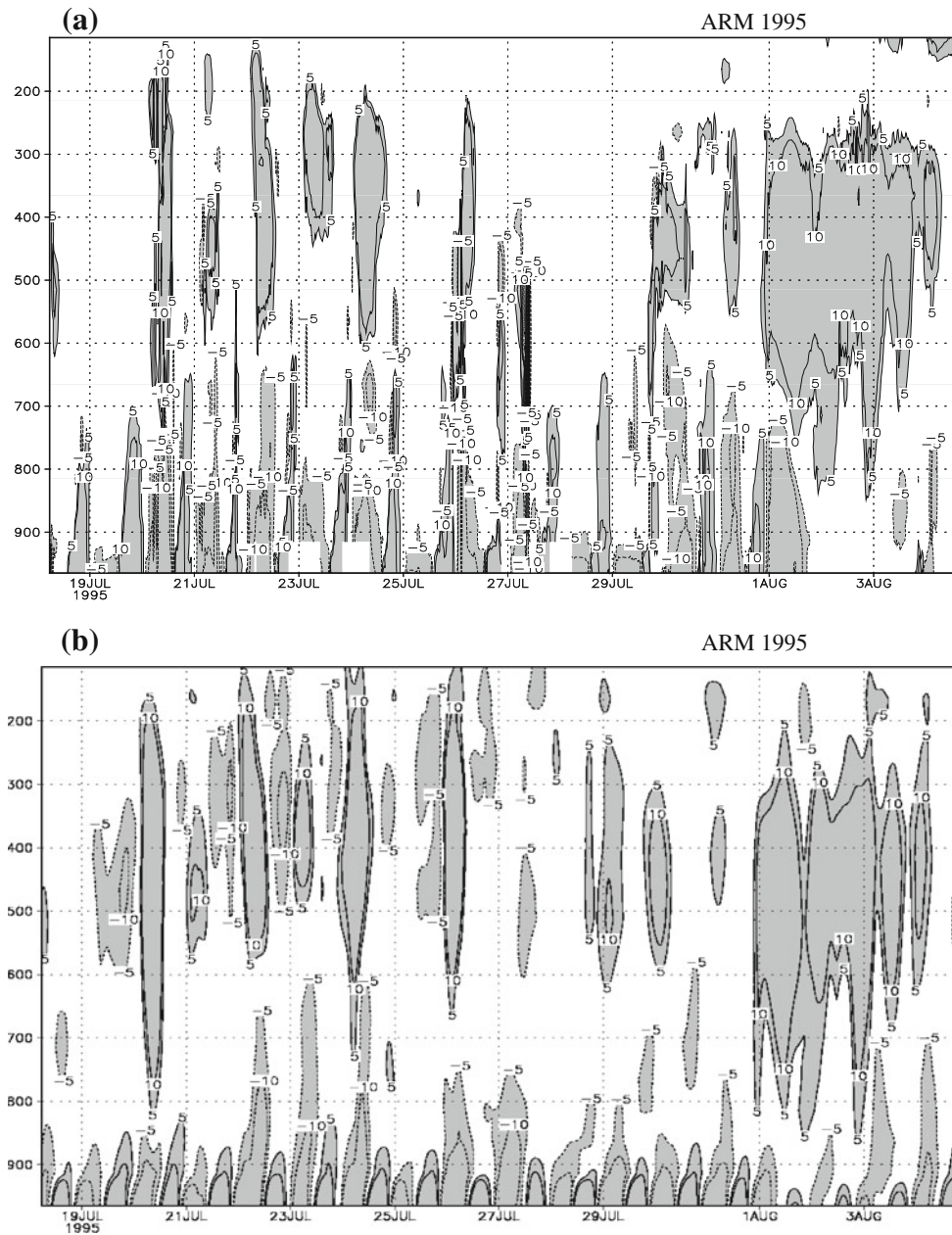


**Fig. 3** Time-pressure cross section of the simulated (a) and observed (b) apparent sources Q1 (K/day) for the ARM 1995 summer IOP

atmosphere by convection is in quasi-equilibrium with destabilization by large-scale forcing in the troposphere. This closure assumption is adopted in our work. Using the convention of Arakawa and Schubert (1974), the net CAPE change can be written as two separated contributions, one due to convective processes and other due to the large-scale processes:

$$\frac{\partial \text{CAPE}}{\partial t} = \left(\frac{\partial \text{CAPE}}{\partial t}\right)_{cu} + \left(\frac{\partial \text{CAPE}}{\partial t}\right)_{ls} \quad (45)$$

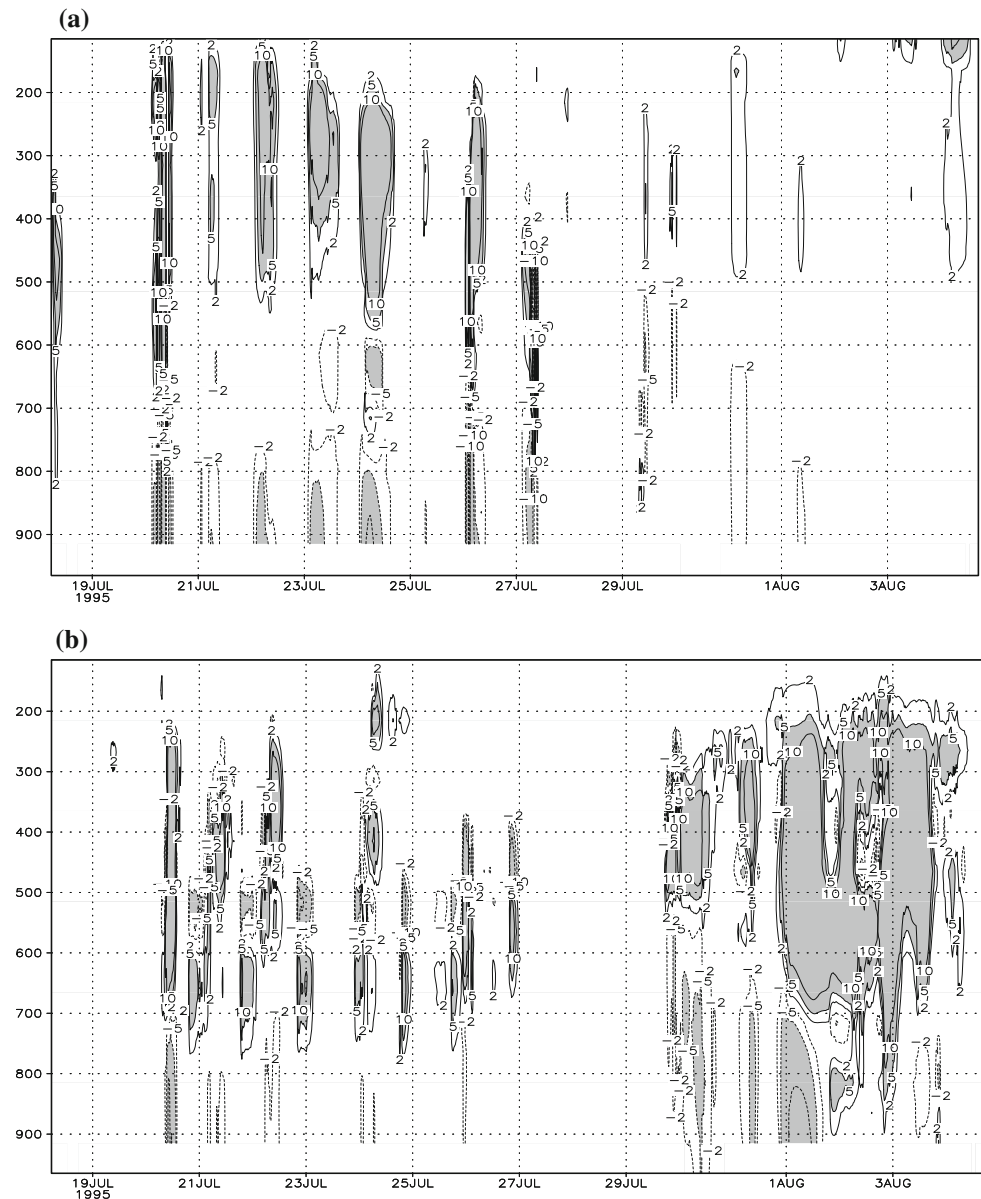
The quasi-equilibrium assumption requires

$$\frac{\partial \text{CAPE}}{\partial t} \ll \left(\frac{\partial \text{CAPE}}{\partial t}\right)_{ls} \quad \text{and} \quad \left(\frac{\partial \text{CAPE}}{\partial t}\right)_{cu} \approx -\left(\frac{\partial \text{CAPE}}{\partial t}\right)_{ls} \quad (46)$$

So, the closure can be written as

$$\int_{p_t}^{p_b} \left[\frac{\partial T_v}{\partial t}\right]_{cu} d \ln p = \max \left\{ -\int_{p_t}^{p_b} \left[\frac{\partial T_v}{\partial t}\right]_{ls} d \ln p, 0 \right\} \quad (47)$$

**Fig. 4** Time-pressure cross section of the simulated heating rate (K/day) for the ARM 1995 summer IOP from **a** Wu's deep convection scheme and **b** the shallow/middle convection scheme of Hack (1994)



Since the temperature change due to convection in the convective layer is proportional to the cloud base mass flux, we have:

$$M_b = \frac{1}{F} \max \left\{ - \int_{p_i}^{p_b} \left[ \frac{\partial \overline{T}_v}{\partial t} \right]_{ls} d \ln p, 0 \right\}. \quad (48)$$

where  $F$  is a proportionality factor. More details can be found in Zhang (2002).

### 3 Numerical tests on single column datasets

The Single-Column Model (SCM) is an important approach used to test and develop parameterizations

(Browning 1994; Randall et al. 1996; Xie et al. 2002; Xu et al. 2002). The new cumulus parameterization suggested in this work is applied to a SCM which is developed by National Center for Atmospheric Research (NCAR) SCM group (Hack and Pedretti 2000) and represents a grid column of a general circulation model (GCM).

In the SCM, the large-scale forcing is prescribed from observations and the moist-convective processes are predicted, thus it has an advantage to isolate cumulus parameterization from the rest. The prognostic equations of temperature and moisture are expressed as

$$\frac{\partial T}{\partial t} = T_{HLS} - \omega \left( \frac{\partial T}{\partial p} + \frac{RT}{pc_p} \right) + T_{phy} \quad (49)$$



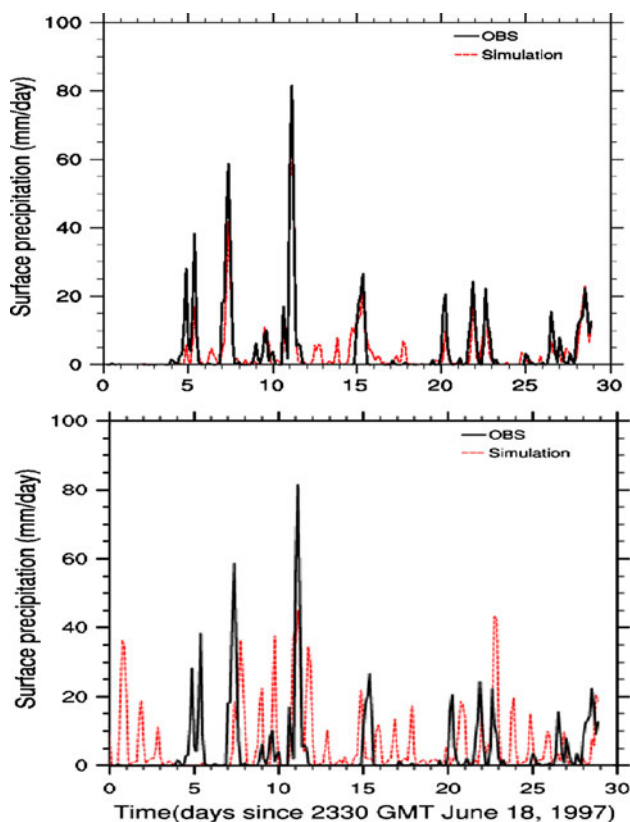


**Fig. 5** The same as that in Fig. 2, but for observed and simulated surface precipitation rates during summer 1997 of the ARM program

$$\frac{\partial q}{\partial t} = q_{HLS} - \omega \frac{\partial q}{\partial p} + q_{phy} \tag{50}$$

where  $T$ ,  $q$ , and  $\omega$  are the temperature, mixing ratio of water vapor, and pressure vertical velocity, respectively. The terms  $T_{HLS}$  and  $q_{HLS}$  represents the large-scale horizontal advective forcing terms.  $c_p$  is the specific heat at constant pressure. The terms  $T_{phy}$  and  $q_{phy}$  show the collection of parameterized physics terms. In the SCM, the terms  $T_{HLS}$  and  $q_{HLS}$  are specified from observations. The vertical advective terms  $-\omega \left( \frac{\partial T}{\partial p} + \frac{RT}{pc_p} \right)$  and  $-\omega \frac{\partial q}{\partial p}$  are calculated by using the observed vertical velocity and predicted temperature and water vapor mixing ratio profiles in the SCM. The surface pressure  $p_s$  and its tendency with time are specified from observations. The basic fields of the prescribed large-scale forcing are interpolated to model levels.

Physical parameterizations in the SCM are the same as those in the NCAR Community Atmosphere Model (CAM3, Collins et al. 2004) except for the deep penetrative convection scheme suggested in this paper (hereafter Wu’s scheme) is applied to replace the original deep convection scheme of Zhang and McFarlane (1995, hereafter ZM’95). For convenience, the original SCM is specified as the NCAR CAM3 SCM and a detailed description can be found in Collins et al. (2004).

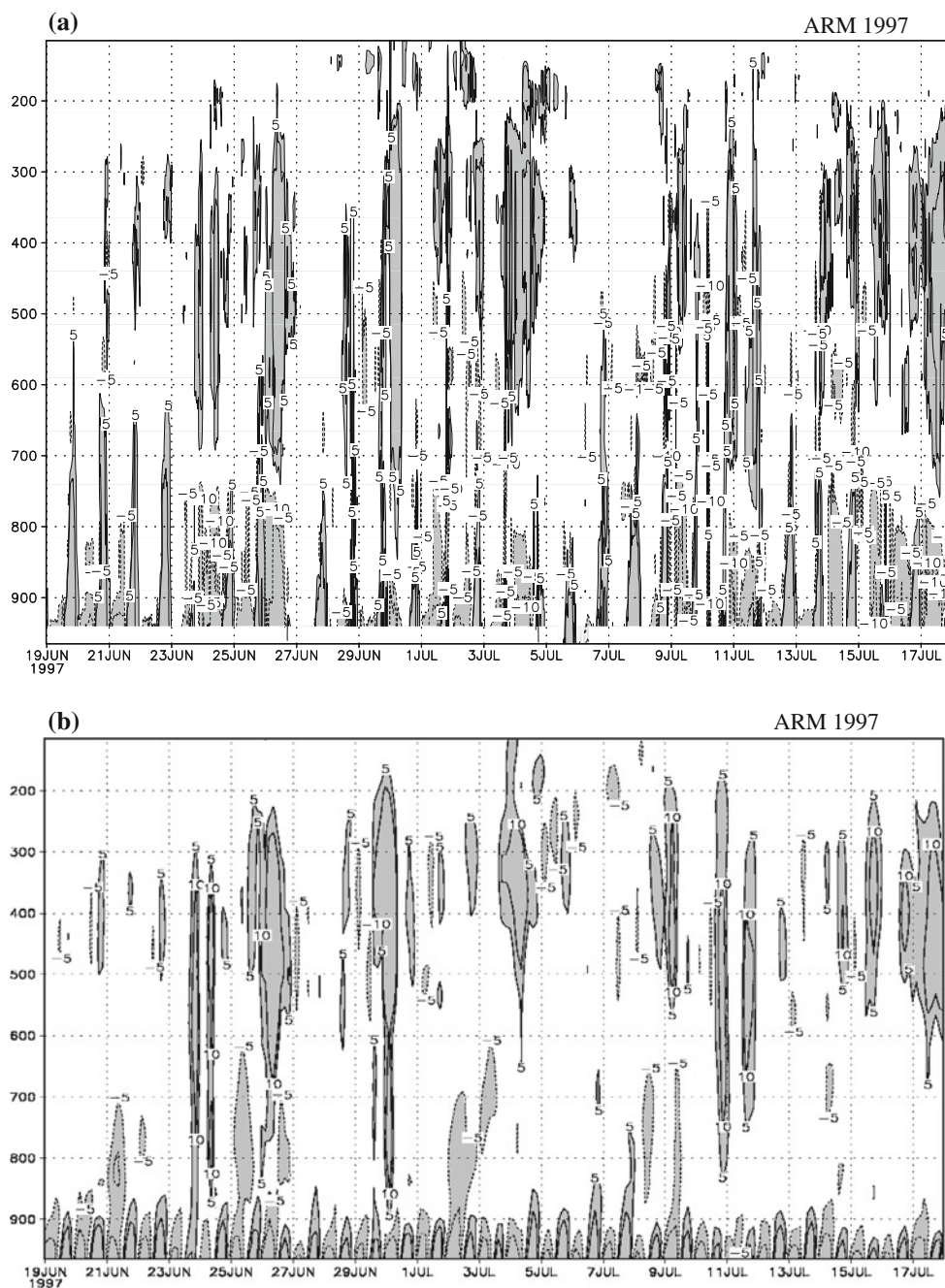
It should be stressed that feedbacks between the convection and the large-scale flow are excluded in the SCM and the tests can only be considered as the validation of a cumulus parameterization. In this work, the data used to force SCM are obtained from the Atmospheric Radiation Measurement (ARM) Southern Great Plains (SGP) site during two intensive operational periods (IOPs) in the summers of 1995 and 1997, and the Global Atmospheric Research Program’s (GARP’s) Atlantic Tropical Experiment (GATE) in year 1974, and the Tropical Ocean and Global Atmosphere Coupled Ocean–Atmosphere Response Experiment (TOGA COARE) from 5 December 1992 through 12 January 1993. In order to make a comparison, integrations of the original NCAR CAM3 SCM in which the ZM’95 deep convection scheme is used are also carried out.

### 3.1 Simulations at ARM Southern Great Plains site

The summer 1995 intensive observing period (IOP) at SGP covers 16 days from 18 July to 3 August 1995. It experienced a wide range of summertime weather conditions and included several intense precipitation events associated with a stationary, large-scale upper-level trough over North America in the first half of the period, and then followed by a few clear days associated with an upper-level ridge (Xie and Zhang 2000). Initial conditions and the time-dependent large-scale forcing terms are obtained from the variational analysis of Zhang and Lin (1997) using surface flux estimates derived from the ARM Energy Balance Bowen Ratio stations (Hack and Pedretti 2000). The large-scale data at the 20-min interval resolution from their analysis are used to compute the needed fields. These fields are then averaged over each 3-h period to obtain the final results. The vertical resolution of the data is 50 hPa from 965 to 115 hPa.

As shown in Fig. 2a, several intense convective precipitation events were observed during the summer 1995 IOP. The SCM captures almost all events of the observed precipitation especially at the beginning and ending of the period. But the simulated precipitation maximum in days 2 and 14 (accounted from 18 July 1995) are obviously smaller than observations. This may be partly attributed to observation errors. In fact, as shown in Figure 6 of Zhang et al. (2001), for all the two intense precipitation events, the rainfall amount averaged over the eight surface meteorological observational stations within the SGP analysis domain is systematically larger than that averaged over the 77 Oklahoma and Kansas Mesonet stations within the same domain. The simulation from the original CAM3 SCM using the same forcing data is shown in Fig. 2b and there are more frequent precipitation events than the observations. The obvious phase shifts between the simulated

**Fig. 6** Same as in Fig. 3, but for the ARM 1997 summer IOP



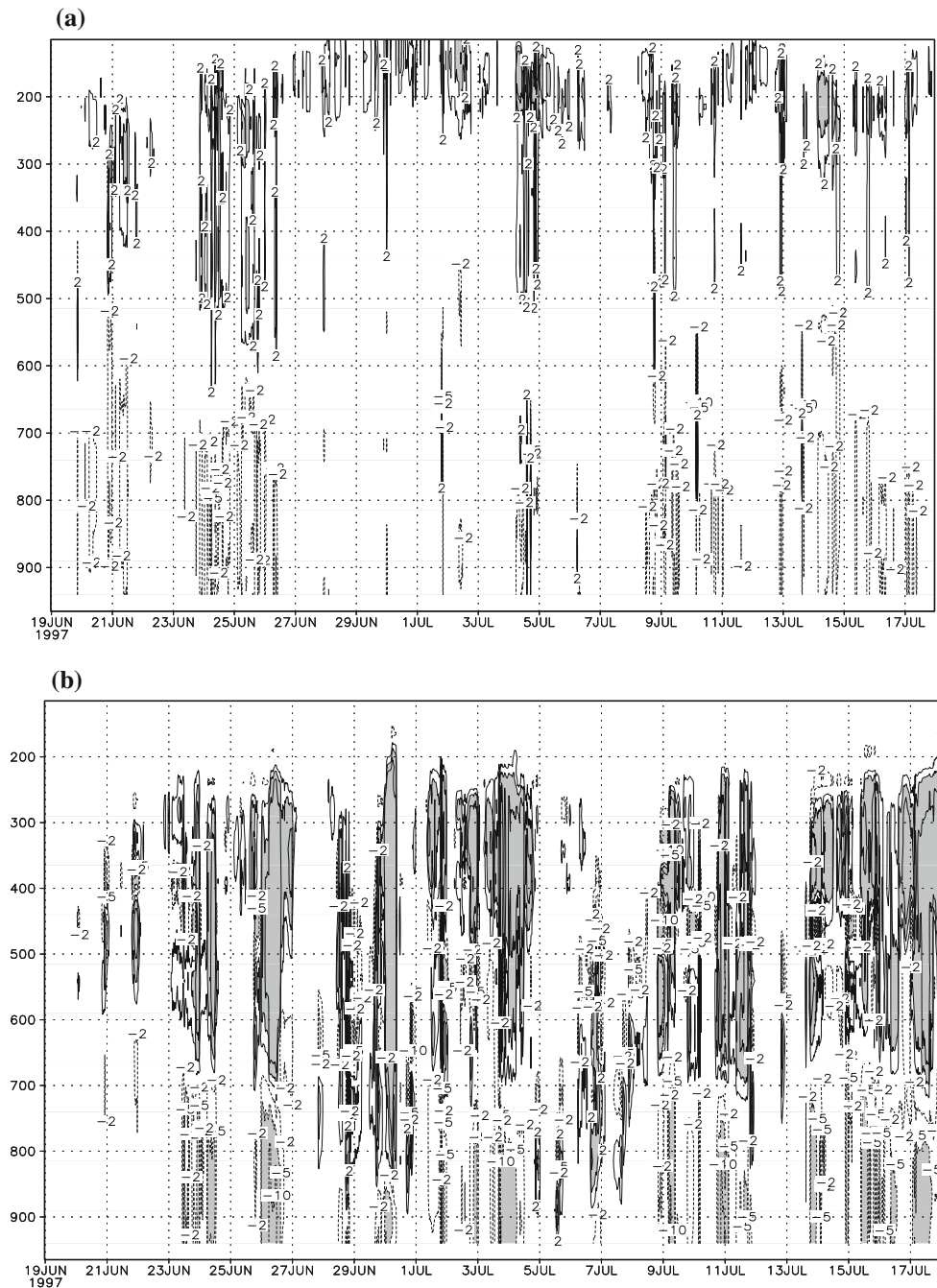
precipitation and the observed precipitation as shown in Fig. 2b also exist in similar simulations of Xie and Zhang (2000) by using the NCAR CCM3 SCM in which the same deep convective scheme of ZM'95 is used. Xie and Zhang (2000) pointed out that the triggering function in the ZM'95 scheme was one of the major causes for the simulation biases.

Figure 3 presents time-pressure sections of the observed and simulated apparent heat sources (Q1, Yanai et al. 1973) over the period of IOP 1995. The vertical profile of simulated Q1 (Fig. 3a) resembles well to the observed Q1 (Fig. 3b). The vertical position and timing of the heating

maxima are generally captured, although the SCM fails to reproduce the heating as strong as observed mainly before 1 August. Furthermore, compared the contribution to the heating rate from the Wu's deep convection scheme with that from the Hack'94 shallow/middle convection scheme (Fig. 4), it can be found that deep convection dominates the moist convection during the period of 20 July to 28 July but after 29 July the shallow/middle convection prevails and deep convection rarely takes place.

The ARM summer 1997 IOP data are also widely used in evaluation of cumulus parameterizations under summertime mid-latitude continental conditions used in SCMs

**Fig. 7** Same as in Fig. 4, but for the ARM 1997 summer IOP



(e.g., Xu et al. 2002; Xie et al. 2002). The summer 1997 IOP covers 29 days from 19 June to 18 July 1997. The data used in the experiment is processed exactly the same manner as those used in the ARM 1995 simulations. The summer 1997 IOP also contained a wide range of summertime weather conditions. As shown in Fig. 5a, the ARM SGP site experienced several intense precipitation events and dry and clear days during this IOP. The SCM captures almost all the main events of observed rainfall for which the maximum surface precipitation is larger than 20 mm/day, including the peaks

of the strong precipitation events. But the SCM also produces several spurious precipitations during non-precipitation periods, especially during days 12–14 but the maximum precipitations are less than 10 mm/day. Figure 5b shows the simulated precipitations from the original CAM3 SCM. The ZM'95 deep convective scheme also produces much more frequent precipitations than the observations as that in 1995 summer. The similar biases in Fig. 5b also exist in the simulations from the NCAR CCM3 SCM (Xie and Zhang 2000).

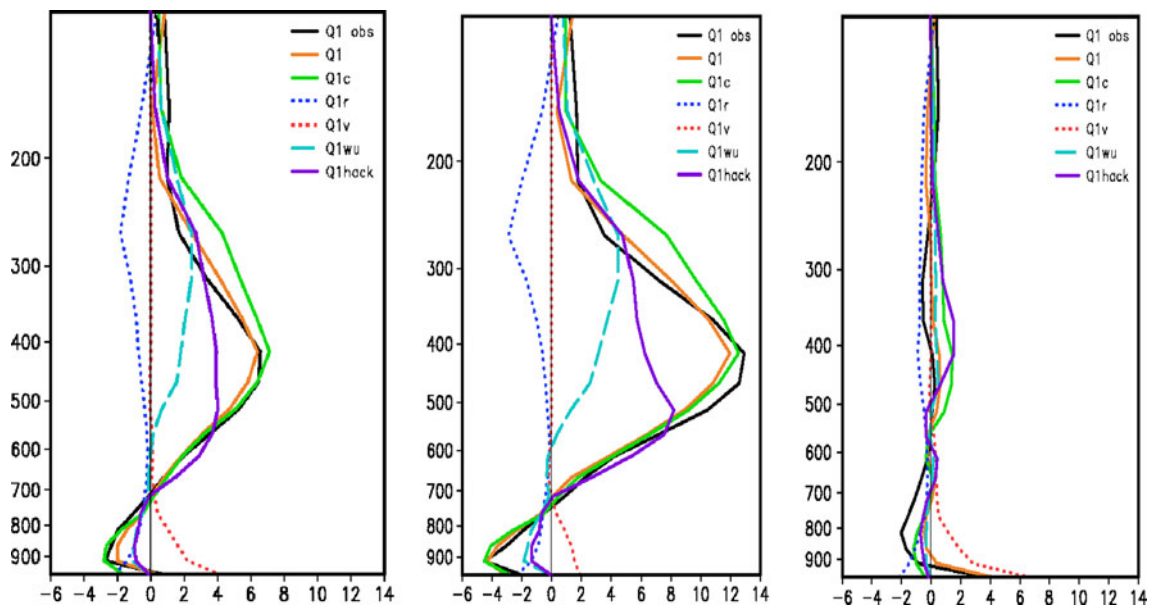


**Fig. 8** Observed and simulated apparent sources ( $Q1$ ) and contributions simulated from total moist convection ( $Q1c$ ), Wu's deep convection ( $Q1wu$ ), Hack shallow/middle convection ( $Q1hack$ ), radiation ( $Q1r$ ), and turbulent processes ( $Q1v$ ) averaged over all the

time (*left*), the precipitation periods (observed precipitation rates  $\geq 0.36 \text{ mm day}^{-1}$ , middle), and the non-precipitation periods (observed precipitation rates  $< 0.36 \text{ mm day}^{-1}$ , right) of ARM 1995 summer IOP, respectively. The units:  $\text{K day}^{-1}$

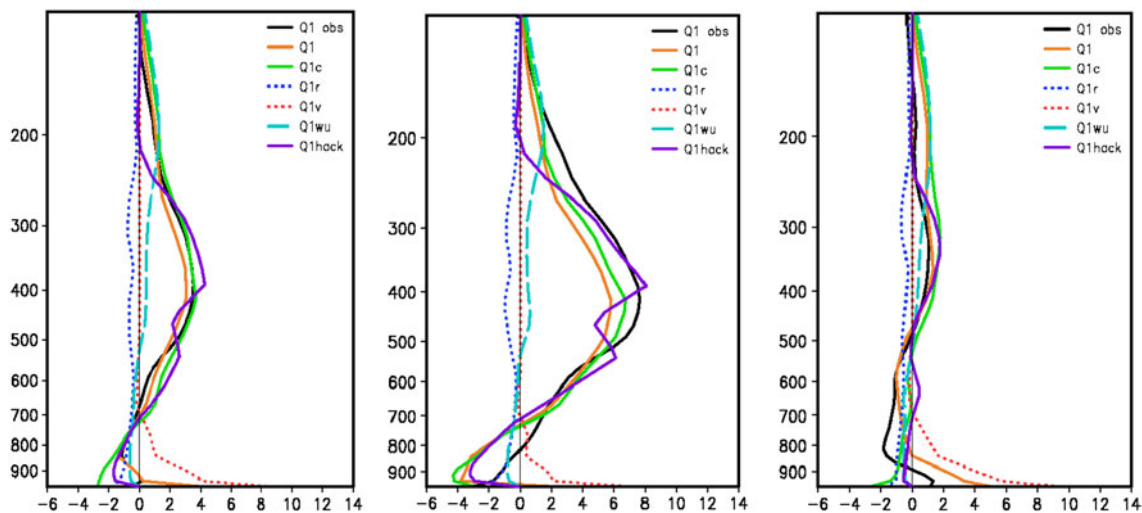


**Fig. 9** Same as in Fig. 8, but for ARM 1997 summer IOP

During the ARM 1997 summer IOP (Fig. 6), the observed  $Q1$  shows heating in the upper troposphere and cooling below about 700 hPa. The SCM can well simulate the vertical profile of observed  $Q1$ . Although the intense precipitation events during this period are also associated with the activities of the large-scale upper-level troughs and ridges over the North American continent (Xie et al. 2002) as that in summer 1995, the convection activities in the SGP site in summer 1997 are different to those in summer 1995. As shown in Fig. 7, the deep convection is obviously weaker than the shallow/middle convection and

the relatively intense deep convection heating is only in the periods of 24–26 June and 4–5 July. The maximum heating from deep convection is located above 500 hPa, up to 200 hPa.

Figures 8 and 9 present time-averaged apparent heat source  $Q1$  and its decomposition for each individual physical processes of total moist convection ( $Q1c$ ), Wu's deep convection ( $Q1wu$ ), Hack shallow/middle convection ( $Q1hack$ ), radiation ( $Q1r$ ), and turbulent processes ( $Q1v$ ) over the periods of IOP 1995 and 1997, respectively. It can be seen that the total  $Q1$  mainly comes from moist

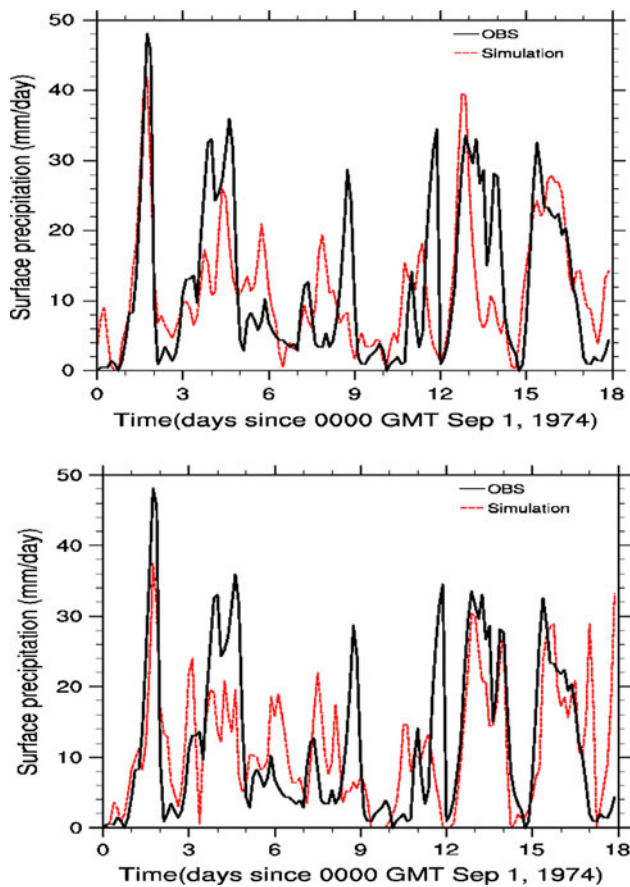


**Fig. 10** The same as that in Fig. 2, but for GATE phase III 1–18 September 1974. *Black line* represents radar observations from Hudlow and Patterson (1979) and manually redrawn from Figure 2 of Piriou et al. (2007)

convective heating (Q1c) in both summers and the vertical profile of simulated Q1 shows a warming in the atmosphere above 700 hPa and a cooling below. If comparing the Q1 between precipitation periods and non-precipitation periods, the precipitation heating to Q1 is more evident. During precipitation periods (Figs. 8b, 9b), the observed Q1 shows strong heating in the upper troposphere and weak cooling in the lower troposphere, but very weak heating and cooling in non-precipitation periods (Figs. 8c, 9c).

In the summer 1995 IOP (Fig. 8), the simulated Q1 is very close to that of the observed Q1. The heating from the Wu's deep convection scheme is mainly located above 600 hPa and reaches its maximum above 300 hPa, and that from shallow/middle convection almost covered from 700 hPa up to above 200 hPa but its maximum is in the lower troposphere. Both of the Wu's deep convection scheme and Hack's shallow/middle convection scheme exhibit a cooling in the atmosphere below 700 hPa. But in the ARM summer 1997 IOP, there is a clear cold bias for the Q1 simulation during the precipitation periods (Fig. 9b) and the strongest Q1 bias in vertical profile is up to

$2 \text{ K day}^{-1}$  in the layer from 500 to 200 hPa. This may be partly attributed to weaker deep convective heating. The heating from deep convection is obviously weaker than that from the shallow/middle convection, especially below 300 hPa. During the non-precipitation time, the Q1 bias is weakened.

### 3.2 Simulations over tropical oceans

It is well known that deep convections over tropical oceans take place frequently. Field experiments such as the GATE and the TOGA COARE provide a large amount of data that can be used to force the SCM (e.g., Emanuel and Zivkovic-Rothmann 1999; Xie and Zhang 2000).

The GATE phase III observations occur in the period from 00Z 30 August to 24Z 18 September 1974 in an experimental area that covers the tropical Atlantic Ocean from Africa to South America. The forcing data are specified in the same way as the ARM experiment. They are on an  $1 \times 1$  degree square grid box with 19 layers from 991.25 to 92.56 mb and cover an area of  $9 \times 9$  degree squares within  $4^{\circ}$ – $14^{\circ}$ N,  $19^{\circ}$ – $28^{\circ}$ W with a observing frequency of 3 h. The SCM integration is for the period from 00Z 1 September to 24Z 17 September 1974.

Figure 10a presents the SCM simulation of precipitation and the reference observed precipitation data that are manually redrawn from Piriou et al. (2007). During GATE phase III observations, the atmosphere experienced robust convective events. This scheme basically reproduces observed precipitation, except for the period of 8–11 September. For a comparison, the simulation from the original NCAR CAM3 SCM is shown in Fig. 10b. The ZM'95 scheme can also capture the main precipitation events in September 2, 3–4, 12–13, and 15–16 of 1974, but produce spurious precipitations in 4 and 17 September. The simulation biases possibly come from early observations over the Atlantic Ocean.

Unlike the SGP site, more frequent deep convection was observed in the tropical Atlantic Ocean. As shown in Fig. 11, the heating from deep convection has a considerable contribution to the Q1 from 900 hPa up to above 200 hPa and the maximum heating is located near 200 hPa. The Hack's middle/shallow convective scheme produces the heating mainly below 300 hPa and the maximum in the lower troposphere between 800 and 500 hPa.

For the TOGA COARE observation in the western tropical Pacific, the SCM simulation is forced by large-scale data averaged from grid points inside the Intensive Flux Array (IFA) during 20–28 December 1992. The IFA domain extends about 700 km in the east–west direction ( $151^{\circ}$ – $158^{\circ}$ E) and about 500 km south–north ( $4^{\circ}$ S– $1^{\circ}$ N). Since the temporal resolution of the dataset is 6 h, a linear interpolation was applied to every model time step.

**Fig. 11** Same as in Fig. 5, but for GATE phase III 1–18 September 1974

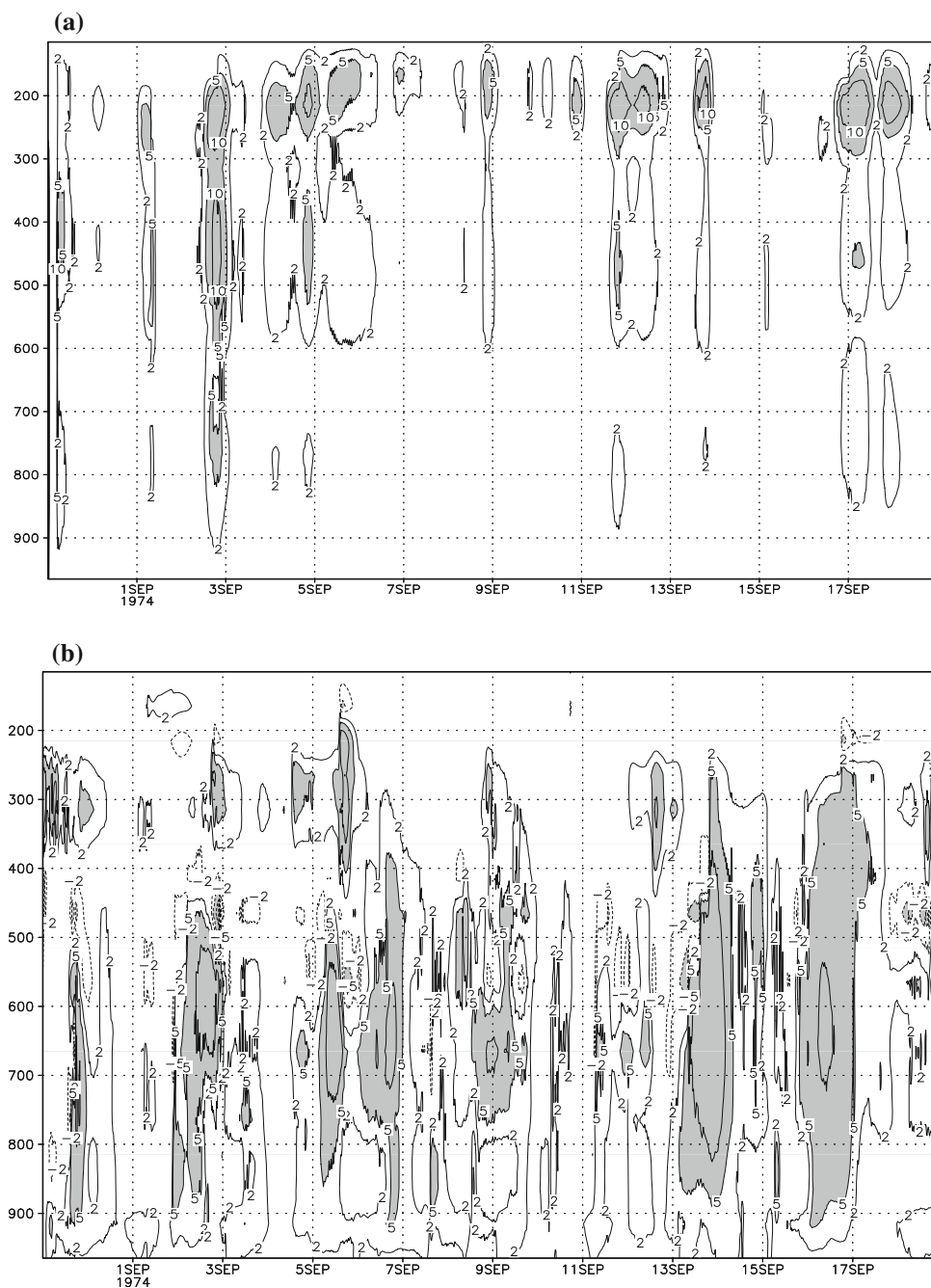
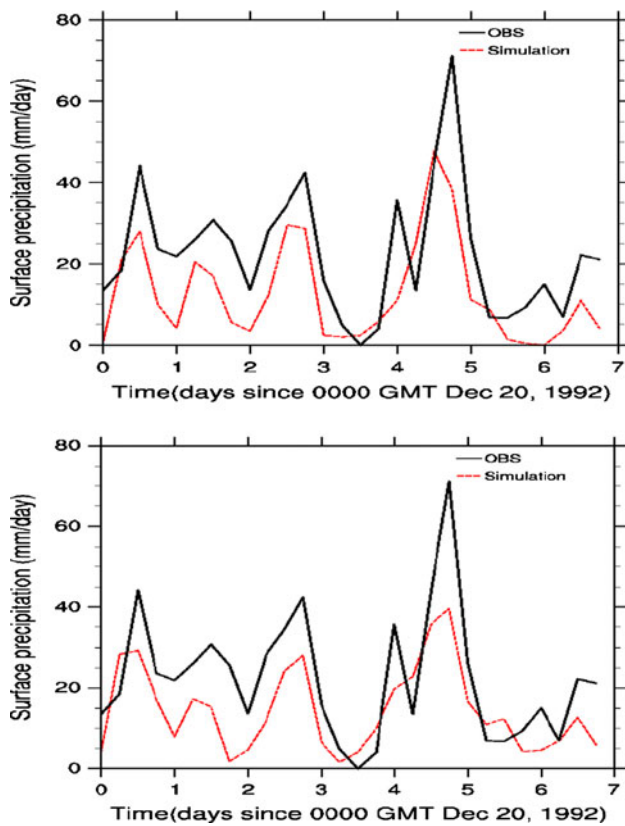


Figure 12a shows the six-hourly rainfall rates produced from a 8-day simulation, as well as the observed rainfall rate that is diagnosed from large-scale budgets (Lin and Johnson 1996) and obtained by combining the vertically-integrated moisture budget residual and the observed surface latent heat flux (from four buoy datasets). The domain of TOGA COARE, in the western Pacific warm pool, is characterized by high sea surface temperatures and strong convective events. During the period of 20–28 December 1992, precipitation occurs almost every day. As shown in Fig. 12a, the SCM can reproduce main characteristics of

the precipitation observed over the warm pool including the beginning, pick, and ending times of each event of precipitation, although the simulated rainfall from the SCM is systematically weaker than the observations. The NCAR CAM3 SCM can also capture the main precipitation events (Fig. 12b) and the simulated precipitation is close to that from the Wu's deep convection scheme.

As shown in Fig. 13, the simulated deep convection in the tropical western Pacific is the thickest cloud column among the three locations, and cloud bottom can start from 850 hPa with the top up to 200 hPa. In the middle to lower



**Fig. 12** The same as that in Fig. 2, but for TOGA 20–28 December 1992

troposphere below 500 hPa, the middle/shallow convection takes the same role as the deep convection in heating the atmosphere.

#### 4 Summary and discussion

This paper has outlined a simple mass-flux cumulus convection scheme and validated it by a SCM. This parameterization scheme is essentially based on the idea of the “bulk” cloud model approach of Yanai et al. (1973), Tiedtke (1989), and Zhang and McFarlane (1995). Properties of the scheme are summarized as follows:

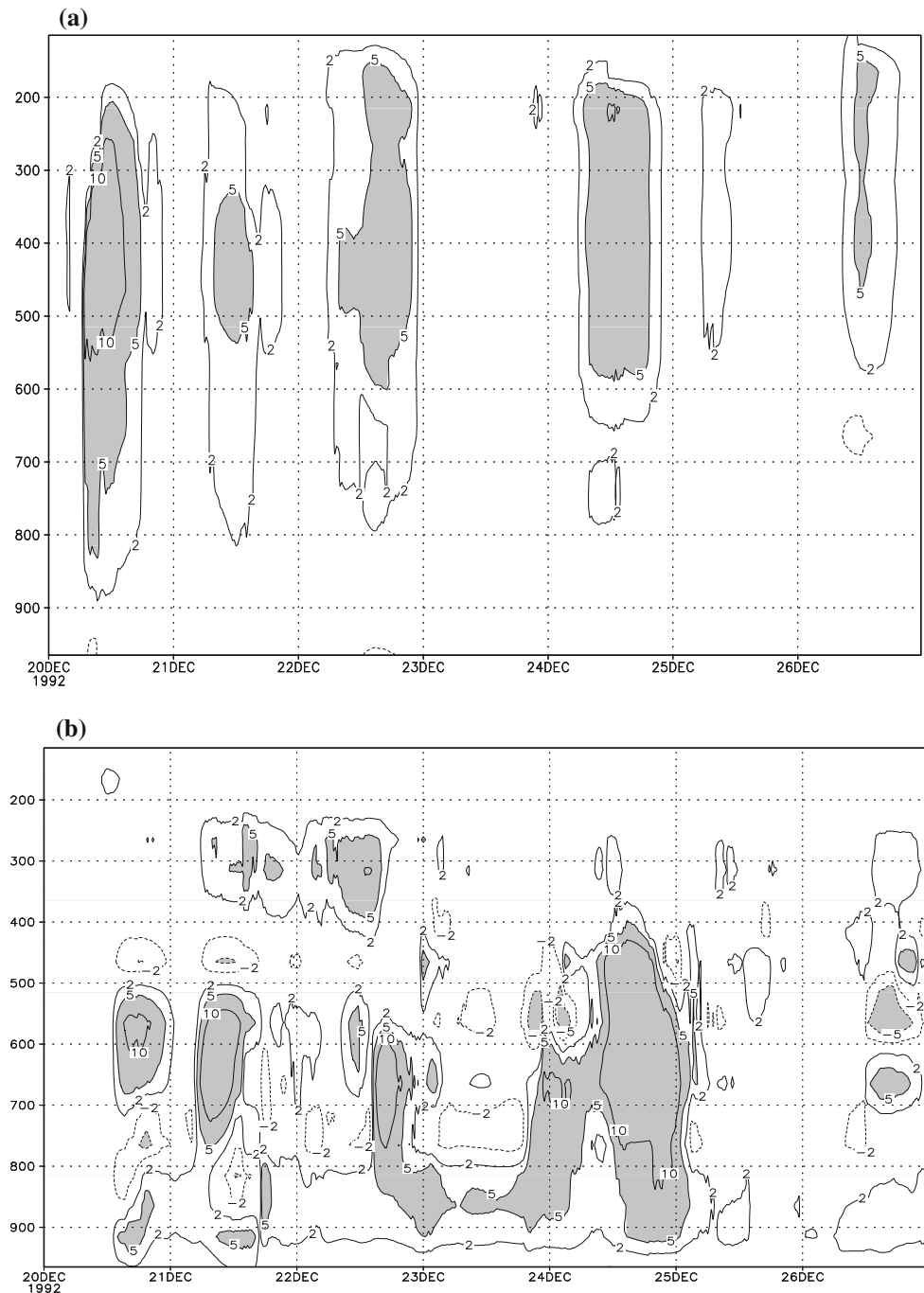
1. Deep convection is triggered when (a) the unstable air parcel at its lifting source level, in which moist static energy above the top of boundary layer approaches its first maximum, is sufficiently moist and the relative humidity is in excess of 75%; and (b) there is positive convective available potential energy.
2. Collective effects of convective clouds on the environmental temperature, moisture, and momentum are taken into account. The cumulus cloud consists of an updraft and a downdraft.

3. The most important process affecting the properties of updraft is mixing or exchange of mass between the updraft cloud parcel and the environment, including the entrainment of the lateral environmental air below the cloud base. The parameterization for entrainment or detrainment of the updraft is different from the commonly-used method that is often a prescribed function with altitude. The entrainment and detrainment are determined by the increase or decrease of cloud parcel mass (or mass flux) with altitude. The cloud mass change with altitude is fully dependent on the properties (e.g., temperature and humidity) of the updraft cloud parcel and the environment, and determined through the total energy conservation for the adiabatic system. The gained energy (including internal thermal energy and the condensation latent heat) for the updraft cloud parcel when there is entrainment of environmental air into cloud is equal to the lost energy for the environment. Similarly, the lost energy (including internal thermal energy and the evaporation latent heat) for the updraft cloud parcel when there is detrainment from cloud parcel is equal to the gained energy for the environment.
4. The convective downdraft parameterization resembles to the scheme used in Zhang and McFarlane (1995). It is assumed that the downdraft originates from the level of minimum environmental saturated equivalent potential temperature and always maintains saturated.
5. The closure assumption proposed by Zhang (2002) is used to determine the mass flux at the cloud base, in which it is calculated from the function of destabilization of the free troposphere due to the free tropospheric temperature and moisture changes caused by large-scale processes.

Based on the observations from the ARM 1995 and 1997 IOP at subtropical continent SGP site and the GATE and TOGA COARE experiments over tropical oceans, the new cumulus parameterization scheme is evaluated by using the SCM developed by NCAR in which the original cumulus convective scheme of Zhang and McFarlane (1995) was replaced. The simulation shows that the SCM can reasonably reproduce the observed precipitation events. The vertical heating profile and timing of the apparent heat sources  $Q_1$  is generally well captured, but  $Q_1$  is slightly underestimated above 500 hPa. The results show that the SCM also produces several spurious precipitations during dry periods.

In the SCM, there are other two schemes in addition to the Wu’s deep convection parameterization scheme, i.e., the Hack’94 shallow convection parameterization and a prognostic cloud water parameterization (Rasch and Kristjansson 1998) affecting the moist processes. The rainfall simulation

**Fig. 13** Same as in Fig. 5, but for TOGA 20–26 December 1992



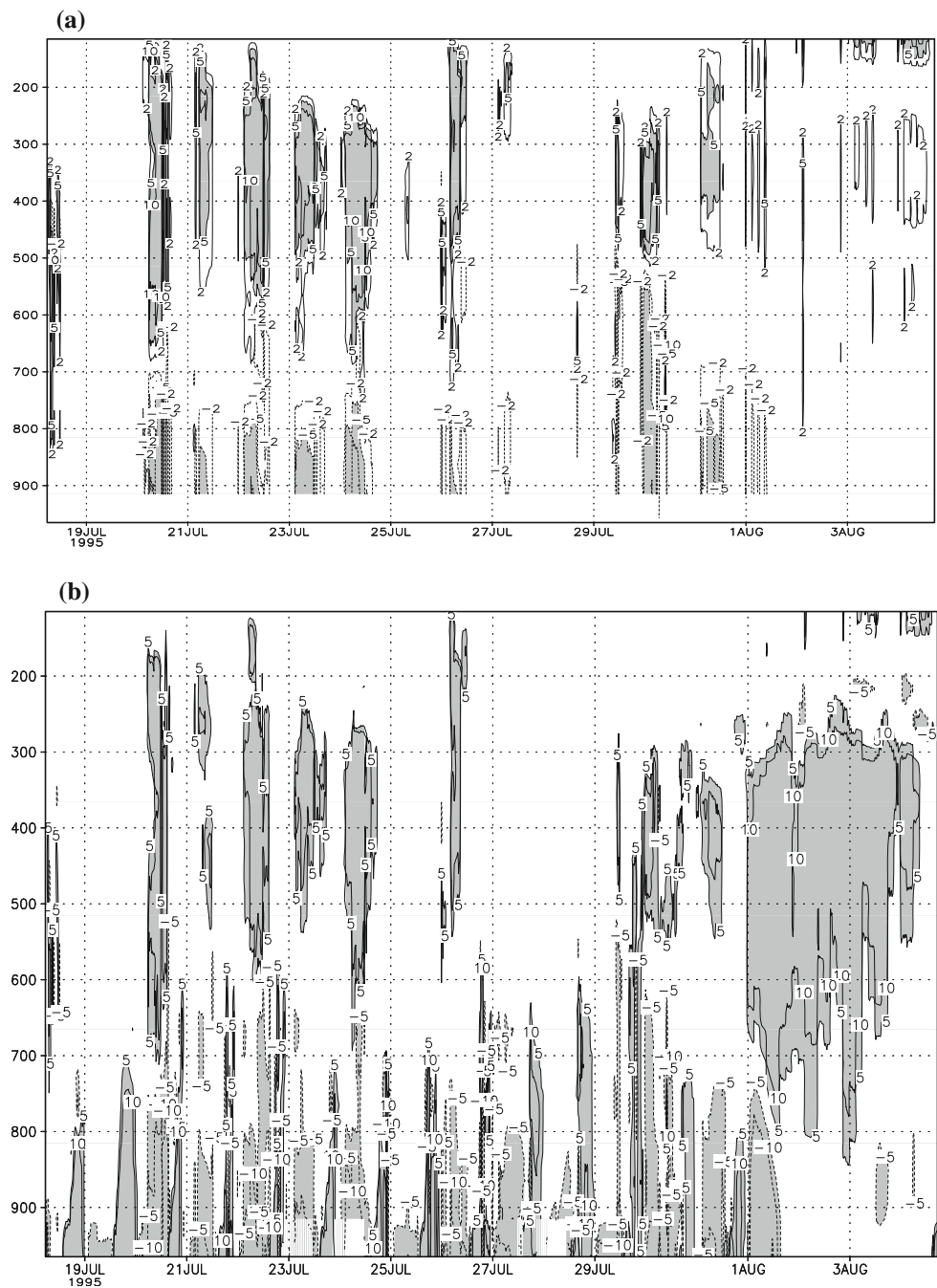
is dependent on not only the presence and acting sequence of the three parameterizations, but also the interaction among them. As shown in Figs. 8 and 9, strong heating produced by deep convection for the ARM 1995 and 1997 summers is generally located in the upper-troposphere and boundary-layer and weak heating in the mid-troposphere, especially between 600 and 700 hPa, that is partly complemented by the Hack's middle/shallow heating (Fig. 4).

Whether the deep convection scheme alone can produce the mid-tropospheric heating is tested through a sensitive simulation using the SCM without the Hack'94 scheme and

the forcing data in the ARM 1995 summer IOP. Simulated deep convective heating rates from the Wu's scheme and the total apparent sources Q1 are presented in Fig. 14. If comparing Fig. 14a with Fig. 4, it can be found that the deep convective activity still centralizes in the period of July 20–26 and the vertical profile of deep convective heating between 600–700 hPa is slightly intensified, but not evident. Only during July 19–31, the deep convection heating in Fig. 14a seems to supplement the middle/shallow convective heating in Fig. 5b. Over the tropical oceans, as shown in Fig. 15, the Wu's deep convective



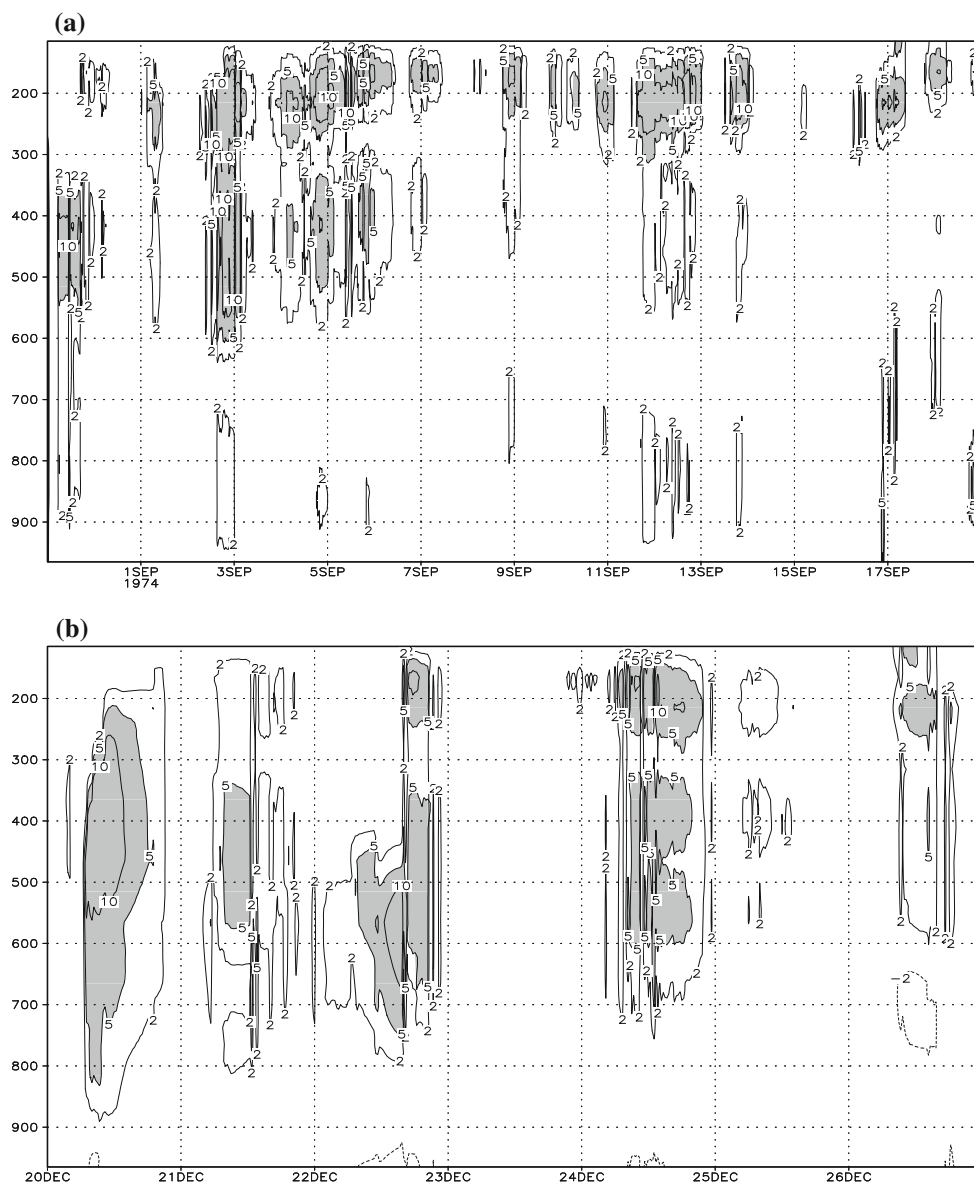
**Fig. 14** Time-pressure cross sections of **a** the simulated deep convective heating rate from the Wu's scheme and **b** the apparent sources Q1 for the ARM 1995 summer IOP when the shallow/middle convection scheme of Hack (1994) is left out. The units: K/day



heating without the Hack's middle/shallow scheme can also partly complement the heating over the lower troposphere. Nevertheless, the deep convective scheme to replace the role of the Hack's middle/shallow scheme in the lower troposphere is still not remarkable. In fact, as the description in Sect. 2, the vertical profile of Wu's deep convective heating is determined by the entrainment or detrainment strength  $\lambda(z)$  which is closely related to the environmental temperature and moisture, and the intensity of deep convective activity is constrained by the closure which depends on the large-scale forcing.

Figure 14b shows time-pressure cross section of the apparent sources Q1 for the ARM 1995 summer IOP when the Hack'94 shallow/middle convection scheme is not activated. With contrast to the Fig. 4b, one can also find the vertical profile of total apparent sources Q1 has no obvious change even if without Hack's middle/shallow scheme, and the Q1 in Fig. 14b resembles to that in Fig. 4b. It exactly accounts for three moist process parameterization schemes in the SCM interacting with each other and relaxing the unstable atmosphere to its stable state.

**Fig. 15** The same as that in Fig. 14, but for the simulated deep convective heating rate from the Wu's scheme for **a** the GATE experiment in 1974 and **b** the TOGA COARE experiment in 1992. The units: K/day



Perfect simulations can not be expected from SCM. Some intrinsic problems can emerge with the SCM approach (Ghan et al. 2000; Hack and Pedretti 2000). Due to the absence of effective internal feedback between the SCM and the large-scale dynamics, the predicted temperature and moisture fields in the SCM can be drifted away from observations after a few days of integration.

A new cumulus convective scheme is designed, in order to improve the performance of GCMs. It has been implemented in the Beijing Climate Center Atmospheric General Circulation Model (BCC\_AGCM2.1) and also in the Beijing Climate Center Climate System Model (BCC\_CSM1.1) which is participating to the phase five of the Coupled Model Intercomparison Project (CMIP5) for IPCC's Fifth Assessment Report (AR5) and has good performance in tropical and subtropical

precipitation simulation. Results from BCC\_AGCM2.1 and BCC\_CSM1.1 will be given in separate studies.

**Acknowledgments** I would like to thank Miss Fang Zhang and Miss Xia Jing for their helps in drawing figures and Dr. Laurent Li and Dr. Baode Chen for constructive comments. This work was supported by the National Basic Research Program of China (973 Program:2010CB951902), the Special Program for China Meteorology Trade (Grant No. GYHY200806006), and the National Natural Science Foundation of China (Grant No. 40928004).

## Appendix

Upon lifting, an air parcel first undergoes dry adiabatic ascent up to its *LCL*. Below the *LCL*, the parcel temperature is

$$T_c = T_{LB} \left( \frac{p}{p_{LB}} \right)^\kappa, \quad (51)$$

where  $k \equiv R_d/c_p$ .  $( )_{LB}$  denotes the variable at the parcel initial level,  $( )_c$  denotes variable of the ascent parcel.  $T$  is temperature in Kelvin,  $p$  is pressure. The parcel humidity mixing ratio does not change during its ascent and there is  $q_c = q_{LB}$ .

Above the *LCL*, the undiluted ascent parcel temperature  $T_c$  and moisture  $q_c$  can be determined following a moist adiabatic process. The equivalent potential temperature  $\theta_e(T_c, q_c, p) = \theta \exp(L_v q_c / c_p T_c)$  is conserved under moist adiabatic processes including phase changes, in which  $\theta$  is the potential temperature,  $L_v$  the latent heat of vaporization, and  $c_p = 1,004.71 \text{ J kg}^{-1}$  the specific heat of dry air. The ascent parcel within cloud is assumed always being saturated, i.e.,  $q_c = q^*(T_c)$ . So, there is  $(\theta_e)_{LCL} = \theta_e^*(T_c)$  where  $(\theta_e)_{LCL}$  is the saturated equivalent potential temperature at the *LCL*, and

$$\theta_e^*(T_c) \equiv T_c \left( \frac{p_{00}}{p} \right)^\kappa \cdot \exp \left[ \frac{L_v q^*(T_c)}{c_p T_c} \right] \quad (52)$$

is the saturated equivalent potential temperature.  $q^*(T)$  denotes the saturated humidity mixing ratio with the temperature  $T$ . If  $(\theta_e)_{LCL}$  is known, the temperature  $T_c$  can be calculated from

$$\theta_e^*(T_c) - (\theta_e)_{LCL} = 0 \quad (53)$$

by Newton–Raphson iteration.

## References

- Anthes RA (1977) A cumulus parameterization scheme utilizing a one-dimensional cloud model. *Mon Weather Rev* 105:270–286
- Arakawa A (2004) The cumulus parameterization problem: past, present, and future. *J Clim* 17:2493–2525
- Arakawa A, Schubert WH (1974) Interaction of a cumulus cloud ensemble with the large-scale environment. Part I. *J Atmos Sci* 31:674–701
- Bechtold P (2006) Atmospheric moist convection. Meteorological Training Course Lecture Series. ECMWF, Shinfield Park, Reading, 74 pp
- Bechtold P, Köhler M, Jung T, Doblas-Reyes F, Leutbecher M, Rodwell MJ, Vitart F, Balsamo G (2008) Advances in simulating atmospheric variability with the ECMWF model: from synoptic to decadal time-scales. *Q J R Meteorol Soc* 134:1337–1351
- Betts AK, Miller MJ (1986) A new convective adjustment scheme. Part II: single column tests using GATE wave, BOMEX, ATEX and arctic air mass data sets. *Q J R Meteorol Soc* 112:693–709
- Browning KA (1994) GEWEX cloud system study (GCSS) science plan. IGPO Publication Series, No. 11, International GEWEX Project Office, 84 pp
- Charney JG, Eliassen A (1964) On the growth of the hurricane depression. *J Atmos Sci* 21:68–75
- Cheng M-D, Arakawa A (1997) Inclusion of rainwater budget and convective downdrafts in the Arakawa–Schubert cumulus parameterization. *J Atmos Sci* 54:1359–1378
- Collins WD et al (2004) Description of the NCAR Community Atmosphere Model (CAM3). Technical Report NCAR/TN-464+STR, National Center for Atmospheric Research, Boulder, Colorado, 226 pp
- Deb SK, Upadhyaya HC, Grandpeix JY, Sharma OP (2006) On convective entrainment in a mass flux cumulus parameterization. *Meteorol Atmos Phys* 94:145–152. doi:10.1007/s00703-005-0175-2
- Donner LJ (1993) Cumulus parameterization including mass fluxes, vertical momentum dynamics, and mesoscale effects. *J Atmos Sci* 50:889–906
- Emanuel KA (1991) A scheme for representing cumulus convection in large-scale models. *J Atmos Sci* 48:2313–2335
- Emanuel KA, Zivkovic-Rothman M (1999) Development and evaluation of a convection scheme for use in climate models. *J Atmos Sci* 56:1766–1782
- Emanuel KA, Neelin JD, Bretherton CS (1994) On large-scale circulations in convecting atmosphere. *Q J R Meteorol Soc* 120:1111–1143
- Fritsch JM, Chappell CF (1980) Numerical prediction of convectively driven mesoscale pressure systems. Part I: convective parameterization. *J Atmos Sci* 37:1722–1733
- Ghan S, Randall D, Xu K-M, Cederwall R, Cripe D, Hack J, Iacobellis S, Klein S, Krueger S, Lohmann U, Pedretti J, Robock A, Rotstain L, Somerville R, Stenchikov G, Sud Y, Walker G, Xie S, Yio J, Zhang M (2000) A comparison of single column model simulations of summertime midlatitude continental convection. *J Geophys Res* 105:2091–2124
- Grabowski WW (2001) Coupling cloud processes with the large-scale dynamics using the cloud-resolving convective parameterization (CRCP). *J Atmos Sci* 58:978–997
- Grabowski WW, Smolarkiewicz PK (1999) CRCP: a cloud resolving convective parameterization for modeling the tropical convective atmosphere. *Phys D* 133:171–178
- Grabowski WW et al (2006) Daytime convective development over land: a model intercomparison based on LBA observations. *Q J R Meteorol* 132:317–344
- Gregory D (1997) The mass flux approach to the parameterization of deep convection. In: Smith RK (ed) *The physics and parameterization of moist atmospheric convection*. Kluwer, Dordrecht, pp 297–320
- Gregory D (2001) Estimation of entrainment rate in simple models of convective clouds. *Q J R Meteorol Soc* 127:53–72
- Gregory D, Rowntree PR (1990) A mass flux convection scheme with representation of cloud ensemble characteristics and stability dependent closure. *Mon Weather Rev* 118:1483–1506
- Gregory D, Kershaw R, Inness PM (1997) Parameterization of momentum transport by convection. II: tests in single column and general circulation models. *Q J R Meteorol Soc* 123:1153–1183
- Gregory D, Morcrette J-J, Jakob C, Beljaars ACM, Stockdale T (2000) Revision of convection, radiation and cloud schemes in the ECMWF integrated forecasting system. *Q J R Meteorol Soc* 126:1685–1710
- Grell AG (1993) Prognostic evaluation of assumptions used by cumulus parameterizations. *Mon Weather Rev* 121:764–787
- Grell AG, Devenyi D (2002) A generalized approach to parameterizing convection combining ensemble and data assimilation techniques. *Geophys Res Lett* 29:381–384
- Hack JJ (1994) Parameterization of moist convection in the National Center for Atmospheric Research Community Climate Model (CCM2). *J Geophys Res* 99:5551–5568
- Hack JJ, Pedretti JA (2000) Assessment of solution uncertainties in single-column modeling frameworks. *J Clim* 13:352–365
- Hu Q (1997) A cumulus parameterization based on a cloud model of intermittently rising thermals. *J Atmos Sci* 54:2292–2307

- Hudlow MD, Patterson VL (1979) GATE Radar Rainfall Atlas. NOAA, Special Report, 155 pp
- Jakob C, Siebesma AP (2003) A new subcloud model for mass-flux convection schemes. Influence on triggering, updraught properties and model climate. *Mon Weather Rev* 131:2765–2778
- Janjic ZI (1994) The step-mountain eta coordinate model: further development of the convection, viscous sublayer, and turbulence closure schemes. *Mon Weather Rev* 122:927–945
- Kain JS, Fritsch JM (1990) A one-dimensional entraining/detraining plume model and its application in convective parameterization. *J Atmos Sci* 47:2784–2802
- Knupp KR, Cotton WR (1985) Convective cloud downdraft structure: an interpretive survey. *Rev Geophys* 23:183–215
- Kuo HL (1965) On formation and intensification of tropical cyclones through latent heat release by cumulus convection. *J Atmos Sci* 22:40–63
- Kuo HL (1974) Further studies of the parameterization of the influence of cumulus convection on large-scale flow. *J Atmos Sci* 31:1232–1240
- Kuo HL, Raymond WH (1980) A quasi-one-dimensional cumulus cloud model and parameterization of cumulus heating and mixing effects. *Mon Weather Rev* 108:991–1009
- Lin X, Johnson RH (1996) Kinematic and thermodynamic characteristics of the flow over the western Pacific warm during TOGA COARE. *J Atmos Sci* 53:695–715
- Lord SJ, Chao WC, Arakawa A (1982) Interaction of a cumulus cloud ensemble with the large-scale environment. Part IV: the discrete model. *J Atmos Sci* 39:104–113
- Manabe S, Smagorinsky J, Strickler RF (1965) Simulated climatology of a general circulation model with a hydrological cycle. *Mon Weather Rev* 93:769–798
- Neggers RAJ, Siebesma AP, Jonker HJJ (2002) A multiparcel method for shallow cumulus convection. *J Atmos Sci* 59:1655–1668
- Ooyama K (1964) A dynamical model for the study of tropical cyclone development. *Geofis Int* 4:187–198
- Piriou J-M, Redelsperger J-L, Geleyn J-F, Lafore J-P, Guichard F (2007) An approach for convective parameterization with memory: separating microphysics and transport in grid-scale equations. *J Atmos Sci* 64:4127–4139
- Randall DA, Xu K-M, Somerville RJC, Iacobellis S (1996) Single column models and cloud ensemble models as links between observations and climate models. *J Climate* 9:1683–1697
- Rasch PJ, Kristjansson JE (1998) A comparison of the CCM3 model climate using diagnosed and predicted condensate parameterizations. *J Climate* 11:1587–1614
- Stensrud DJ, Fritsch JM (1994) Mesoscale convective systems in weakly forced large-scale environments, part III: numerical simulations and implications for operational forecasting. *Mon Weather Rev* 122:2084–2104
- Sun W-H, Haines PA (1996) Semi-prognostic tests of a new cumulus parameterization scheme for mesoscale modeling. *Tellus* 48A:272–289
- Sundqvist H (1988) Parameterization of condensation and associated clouds in models for weather prediction and general circulation simulation. In: Schlesinger ME (ed) *Physically-based modeling and simulation of climate and climate change*, vol 1. Kluwer, Dordrecht, pp 433–461
- Tiedtke M (1989) A comprehensive mass flux scheme for cumulus parameterization in large-scale models. *Mon Weather Rev* 117:1779–1800
- Tompkins AM (2001) Organization of tropical convection in low vertical wind shear: the role of water vapor. *J Atmos Sci* 58:529–545
- Wang J, Randall DA (1996) A cumulus parameterization based on the generalized convective available potential energy. *J Atmos Sci* 53:716–727
- Wang Y, Zhou L, Hamilton K (2007) Effect of convective entrainment/detrainment on the simulation of the tropical precipitation diurnal cycle. *Mon Weather Rev* 135:567–585
- Wu T, Yu R, Zhang F, Wang Z, Dong M, Wang L, Jin X, Chen D, Li L (2010) The Beijing Climate Center atmospheric general circulation model: description and its performance for the present-day climate. *Clim Dyn* 34:123–147. doi:10.1007/s00382-008-0487-2
- Xie SC, Zhang M (2000) Impact of the convection triggering function on the single-column model simulations. *J Geophys Res* 105(D11):14983–14996
- Xie SC et al (2002) Intercomparison and evaluation of cumulus parameterizations under summertime midlatitude continental conditions. *Q J R Meteorol Soc* 128:1095–1135
- Xu K-M et al (2002) An intercomparison of cloud-resolving models with the atmospheric radiation measurement summer 1997 intensive observation period data. *Q J R Meteorol Soc* 128:593–624
- Yanai M, Esbensen S, Chu JH (1973) Determination of bulk properties of tropical cloud clusters from large-scale heat and moisture budgets. *J Atmos Sci* 30:611–627
- Zhang GJ (2002) Convective quasi-equilibrium in midlatitude continental environment and its effect on convective parameterization. *J Geophys Res* 107(D14). doi:10.1029/2001JD001005
- Zhang GJ (2009) Effects of entrainment on convective available potential energy and closure assumptions in convection parameterization. *J Geophys Res* 114:D07109. doi:10.1029/2008JD010976
- Zhang MH, Lin JL (1997) Constrained variational analysis of sounding data based on column-integrated budgets of mass, heat, moisture, and momentum: Approach and application to ARM measurements. *J Atmos Sci* 54:1503–1524
- Zhang GJ, McFarlane NA (1995) Sensitivity of climate simulations to the parameterization of cumulus convection in the Canadian Climate Center general circulation model. *Atmos Ocean* 33:407–446
- Zhang MH, Lin JL, Cederwall RT, Yio JJ, Xie SC (2001) Objective Analysis of ARM IOP Data: Method and Sensitivity. *Mon Weather Rev* 129:295–311